Dalton Transactions

ROYAL SOCIETY OF CHEMISTRY

PAPER

View Article Online
View Journal | View Issue

Cite this: *Dalton Trans.*, 2021, **50**, 2243

Structure-reactivity studies on hypervalent square-pyramidal dithieno[3,2-*b*:2′,3′-*d*]phospholes†

Nayanthara Asok, Joshua R. Gaffen, Ekadashi Pradhan, Tao Zeng * and Thomas Baumgartner *

Received 7th January 2021,
Accepted 19th January 2021

DOI: 10.1039/d1dt00062d

rsc.li/dalton

A series of neutral pentacoordinate dithieno[3,2-*b*:2′,3′-*d*]phosphole compounds were synthesized by [4 + 1] cycloaddition with *o*-quinones. Counter to the expected trigonal bipyramidal geometry, the luminescent hypervalent dithienophospholes exhibit square pyramidal geometry with inherently Lewis acidic phosphorus center that is stabilized *via* supramolecular π-stacking interactions in the solid state and in solution. Due to their Lewis-acid character, the compounds react with nucleophiles, suggesting their potential as mediator in organic transformations. The new species thus present an intriguing structural plaform for the design of neutral P(v) Lewis acids with useful reactivities.

Introduction

Organic conjugated material research is a popular field owing to the practical application of these materials in various devices, such as organic light-emitting devices (OLEDs), organic photovoltaic devices (OPVs), organic field-effect transistors (OFETs), and sensors.[1] While numerous high-performing p-type materials have been developed and are utilized in these devices, the scarcity of corresponding n-type materials demands innovative molecular designs for improved efficiency.[2]

One particularly intriguing area of research towards this goal deals with the development of main group element-containing building blocks.[2c] The unique structural elements and intrinsic electronics of the main group components provide a convenient avenue for effective property tuning, particularly with a view toward organic electronics. A valuable scaffold that is extensively studied in this context is dithieno[3,2-*b*:2′,3′-*d*]-phosphole (**I**, Fig. 1a).[3] The electron-accepting ability of conjugated phospholes arises from σ*–π* hyperconjugation, in which the σ* orbital of the exocyclic P–R bond interacts with the π* orbital of the butadiene moiety to generate a stabilized LUMO level (Fig. 1a).[4] The ease of alteration of the LUMO energy by modification of the P center (R) or the main framework (R′), along with strong fluorescence properties has driven the comprehensive investigation of dithienophospholes as potential material for application in organic electronics.[3b]

While most of the previous work focused on amendment of the electronics by exocyclic substitution reactions, including the functionalization of the phosphorus lone pair,[3b] the alteration of the geometry of the P center as a methodology to influence the energies of the frontier molecular orbitals (FMOs) is relatively less explored.[4–6] An interesting structural platform for this purpose are hypervalent phosphorus compounds with coordination numbers of five or six.[7]

Since trivalent phosphorus species are known to undergo [4 + 1] cycloaddition with *o*-quinones to form pentacoordinate molecules,[8] we were interested in exploring if this approach could be extended to dithienophospholes as well. The Valence Shell Electron Pair Repulsion (VSEPR) model-predicted trigonal bipyramidal (3BP) geometry of the proposed molecule **II** (Fig. 1b) with pentavalent phosphorus exists by virtue of a 3-center-4-electron bond (3c–4e bond, shown in red), with its

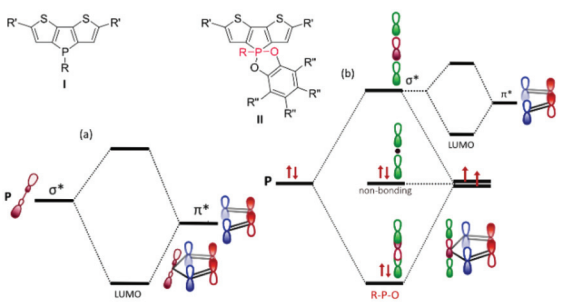

Fig. 1 (a) σ*–π* Hyperconjugation in dithienophosphole; (b) 3c–4e bond in the proposed hypervalent molecules.

Department of Chemistry, York University, 4700 Keele Street, Toronto, ON M3J 1P3, Canada. E-mail: tzeng@yorku.ca, tbaumgar@yorku.ca

† Electronic supplementary information (ESI) available: Synthesis and characterization of the compounds; theoretical calculation details; Reactivity and stability studies, crystallographic data; CCDC 2044241(**A**), 2044242 (**B**), 2044243(**C**), 2044244(**D**) and 2044245 (**A**·H_2O). For ESI and crystallographic data in CIF or other electronic format see DOI: 10.1039/d1dt00062d

three molecular orbitals (MOs) of which the bonding and non-bonding MOs are filled.[9] This non-classical bond would impart the electron-accepting properties by providing a vacant σ* orbital that can interact with the π* orbital of butadiene moiety (Fig. 1b). Importantly, the σ* orbital is oriented perfectly orthogonally to the butadiene moiety and should thus lead to better overlap with the π-system. We expected the hypervalency to be effectively leveraged in generating neutral and stable pentavalent phosphorus compounds with enhanced electron-accepting abilities compared to that of their parent trivalent analogue.

To our surprise, however, many unexpected observations, chiefly the generation of square pyramidal (4SQ) structures, arose during the course of this study, and we were afforded with an intriguing opportunity to shift our focus with these new species. Pentacoordinate phosphorus in a 4SQ geometry is uncommon, but not unprecedented.[10] However, literature largely only provides a nebulous description of what dictates the geometry of such species. Structural assignments are generally based on a competing mixture of steric forces and undefined electronic arguments, using the withdrawing nature of the phosphorus substituents.[10a–c,11] While the reported 4SQ systems do result in Lewis-acidic neutral phosphorus species,[12] the studies do not strictly afford an understanding of the electronic requirements for a 4SQ P(v) center. For better insight into that question, one can look into the heavier congeners of stibanes. Antimony pentahalides are well known Lewis acids, but several typical pentacoordinate Sb(v) species have nebulous geometric configurations.[13] Even the simple $SbPh_5$ exhibits a distorted 4SQ geometry.[13a,b] Counterintuitively, the perhalogenated species $Sb(C_6X_5)_5$ exhibit a fairly regular 3BP geometry, as typically a more withdrawing substituent is presumed to enforce a 4SQ geometry in phosphorus species.[13c] The $SbPh_5$ geometry is proposed to exist in the solid state due to the isoergic nature of the 3BP and 4SQ geometries, yet this similarity in energy is not quite understood.[13a,b] Finally, a related series of heterobicycles reported by Holmes *et al.* strictly exhibits 4SQ geometry, highly reminiscent of the new series of structures reported herein.[13d,e]

With this contribution, we investigate what ultimately dictates the geometric orientation of these species, and what impact does that have on the inherent Lewis acidity of the phosphorus center. To this end, we report the synthesis, structures, properties, and reactivity of the new hypervalent dithienophospholes that provide an exciting opportunity for understanding these types of system more deeply.

Results and discussion

Synthetic procedures

For our study, we focused on species that would potentially be able to (a) stabilize the hypervalent state and/or (b) enhance the electron-acceptor properties of the target species. To this end, we identified *o*-chloranil and phenanthrene quinone as suitable quinones, while the phenyl- and perfluorophenyl-substituted **1**[3a] and **2**[14] were our dithienophospholes of choice.

An equimolar solution of compound **1** and *o*-chloranil in degassed, dry DCM (MBraun SPS) afforded compound **A**, which was isolated after column chromatography (Silica, DCM) in 63% yield (Scheme 1). The same reaction conditions worked well for the perfluorophenyl phosphole **2** with *o*-chloranil and phenanthrene, resulting in the isolation of compounds **C** in 62% yield and **D** in 80% yield, respectively. A similar equimolar reaction of compound **1** and phenanthrene quinone was initially conducted in refluxing THF as the solubility of the quinone was better in this solvent. Even though the reaction exhibited a new phosphorus species after 20 hours, later revealed to be compound **B**, upon isolation only the starting material **1** and corresponding oxide **3** were detected. We thus revisited synthesis of **B** with meticulously dried DCM (degassed DCM, dried by passing through activated neutral alumina, followed by three cycles of freeze-pump-thaw). Using these conditions, compound **B** was successfully synthesised in a glovebox and isolated by crystallization from toluene in 61% yield. The successful generation of the 5-coordinate species was indicated by the shift in fluorescence emission (see ESI†) and a significant highfield shift of the ^{31}P NMR resonances, consistent with a 5-coordinate phosphorus(v) center.[15]

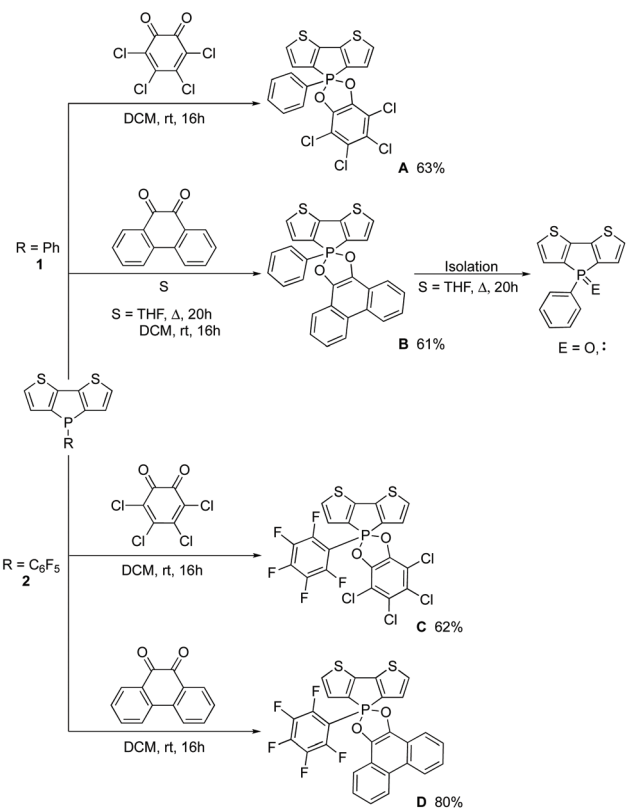

Scheme 1 Synthesis of quinone-functionalized hypervalent dithienophospholes.

Solid state characterization

Single crystals suitable for X-ray diffraction were readily grown from compounds **A**, **C**, and **D** and with some difficulty of compound **B**. Rather unexpectedly, all the structures exhibited a distorted square pyramidal (4SQ) geometry (Fig. 2) as opposed to the more typical, and VSEPR supported 3BP geometry containing a 3c–4e bond (Fig. 1b).

The central phosphorus atom is moved out of the plane of the π-conjugated scaffolds by approximately 0.4 Å, with the aryl groups (phenyl for **A** and **B**, perfluorophenyl for **C** and **D**) arranged nearly orthogonally to the plane containing the quinone unit and dithienophosphole moiety (angles are 103.7(7)°, 103.6(5)°, 105.6(2)° and 103.2(4)° **A**, **B**, **C**, and **D**, respectively) to form the apex of the square pyramid.

While the average P–C bond lengths in these structures (1.8 Å) are very close to usually observed P–C bond lengths of 1.84 Å,[16a] the P–O bonds are elongated to 1.7 Å from normally observed P–O bond lengths of 1.63 Å,[16b] but consistent with a catecholate chelating to a P(v) center.[10f,g,i]

Precedent for these structures, albeit uncommon, is found in the literature,[10b] but previous studies do not afford a clear explanation of what constrains such systems to this 4SQ geometry. While the related 3BP structures predominantly orient the substituents about the phosphorus center to afford the most favorable 3c–4e bonds, a similar argument is not obviously applicable to the 4SQ equivalent species.[10c] While it has been suggested that a strong electron-withdrawing ligand will instil 4SQ geometry,[10a,11] that is not often the case; oxalates and tetrachlorocatecholates readily afford 3BP structures, as found in chirality resolution agents.[17] The 4SQ geometry can also be enforced *via* geometric constraints;[10a,b,11] Holmes *et al.* leveraged the strain of a 4-membered ring to offset the presumably higher-energy 4SQ geometry.[10f] Gilhula and Radosevich employ tetradentate or scorpionate ligands to enforce a 4SQ geometry in order to make use of the reactivity of the 4SQ phosphorus center in chemical transformations.[18] Our species, however, consist instead of a catecholate and phosphole. The bite angle of the 1,2-diol system is geometrically restrictive. The resultant 5-membered ring with the phosphorus center exhibits a nearly 90° O–P–O bond angle. However, while catecholates form strong chelates with P(v) centers, they are often labile, detaching and reattaching to afford the preferred geometric isomers;[19] and even allow for the generation of reactive sites at either the unbound P or O atoms. These available sites are short lived, however, and are typically observed only if captured, such as by a silyl group or cation for O^- or a base such as F^- for P^+, to prevent the re-association of the oxygen with the phosphorus center.[19] With respect to the phosphole unit, while breaking a P–C bond within the phosphole is not entire impossible, it is a less labile substituent than the catecholate. In addition, the geometry of the C–P–C unit of the phosphole ring is not dictated by, for example, like above the strain of a 4-membered ring system, but the electronic interactions between the phosphorus center, the diene system and the exocyclic substituents. Our system would therefore, intuitively, generate the most favorable isomer in solution due to the lability of the catecholate and the geometry at the phosphole being dictated by the association of said catecholate, when compared to these structures of precedent.[19] Still, the small bite angle of the catecholate prohibits the formation of the most favourable 3c–4e bond, an O–P–O bond, in which the optimized 3BP structure is formed by the axial oxygen donating a lone pair into the opposing σ^*_{PC} orbital, requiring instead a weaker 3c–4e C–P–O bond between one catecholate oxygen and one *ipso*-carbon to retain a 3BP structure. To better understand the complex interplay between these factors, we turned our focus to computational chemistry. A detailed analysis of the 3BP *vs.* 4SQ structural preference is given in section 9(i) of the ESI† using compound **A** as a representative species.

The natural bond orbital (NBO) population analysis[20] shows expected electron transfer from phosphorus to both oxygen atoms, with natural atomic charges of +1.90 and −0.75 for P and O atoms, respectively. Both oxygen atoms, somewhat unexpectedly, are available to donate a lone pair to their opposite σ^*_{PC} orbitals to generate two 3c–4e bonds. In the 3BP structure, one strong formal 3c–4e bond exists between the axial O and the axial C(*ipso*), while in the 4SQ structure, two symmetrically equivalent 3c–4e bonds persist in the square base. Our calculation shows that the conversion from the 3BP to the 4SQ structure involves the process of weakening the 3c–4e bond of the 3BP isomer, relaxing the 120° bond angles between the equatorial substituents, and developing a second 3c–4e bond. This energy compensation results in comparable stabilities of the 3BP and 4SQ structures, and thus their dynamic sampling in solution.[7b,10b,21] Since the 4SQ structure is in-between two 3BP structures (each having one or the other O atom at the axial position), the sampling results in an averaged 4SQ structure, which is observed in our structural characterizations. In the solid state, 4SQ structures are exclusively observed because their parallel arrangements of the extended conjugated scaffolds between adjacent molecules also enhances their π–π stacking interactions (*vide infra*). As such

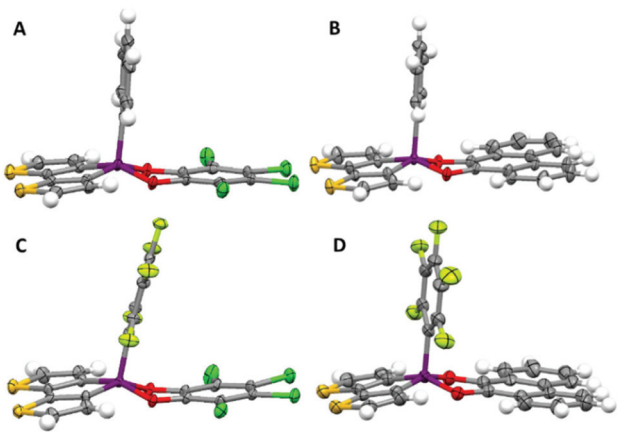

Fig. 2 Molecular structures of compounds **A**, **B**, **C**, and **D** in the solid state. Ellipsoids are set at 50% probability.

the ability to generate stable 4SQ species relies on generating two 3c–4e bonds of intermediate strength that afford the system similar stability as the strong 3c–4e bond of the 3BP isomer. This process may be performed either electronically, geometrically, or both as long as the resultant 3c–4e bonds of the 4SQ isomer are sufficiently strong so as to afford an isoergic isomer to the 3BP structure. This explanation can be seen in the computational analysis of structures **A–D**, whose energy differences between the two isomers are −0.4, 0.1, 1.7, and 1.1 kcal mol^{-1}, respectively (negative means 4SQ being more stable). With the small energy differences, the molecules in fact likely dynamically rock between the 3BP and 4SQ structures (akin to Berry pseudorotation),[7b,10b,21] affording some insight into the aforementioned dynamic solutions state nature of these compounds. This dynamical rocking reflects the lability of the bidentate interaction between P and the catecholate O atoms, despite their rigid O–P–O angle. Such an in-depth analysis of the preference towards 4SQ structure of a P(v) structure has not been previously explored. Note that, as expected, compounds **C** and **D** exhibit slightly more favorable 3BP geometric isomers. But this is not due to the more electronegative C_6F_5 group, which always occupies an equatorial position in the 3BP structures.

Reactivity studies of the hypervalent compounds

We surmised that the unexpected 4SQ geometry could also impart intriguing reactivity to these hypervalent compounds, similar to related species in the literature,[22] as suggested by the electron-density mapping (Quantum Theory of Atoms in molecules; QTAIM) representatively on compound **A**.[23] An area of low electron density on the P center, often referred to as sigma hole,[24] is a potential coordination site for nucleophiles such as OH^- or F^-, which would make these hypervalent compounds neutral Lewis acids (Fig. 3a).[12] Recent examples of such rare neutral Lewis acids, include the bis(perchlorocatecholato)silane (**IIIA**) with a Lewis-acidic Si(IV) center, reported by Greb *et al.*[12d,e] This compound has been classified as Lewis Super Acid by virtue of its high fluoride ion affinity (FIA; 507 KJ mol^{-1}) and acquires similar square pyramidal geometry on abstraction of a fluoride anion (**IIIB**) (Fig. 3b).[12d]

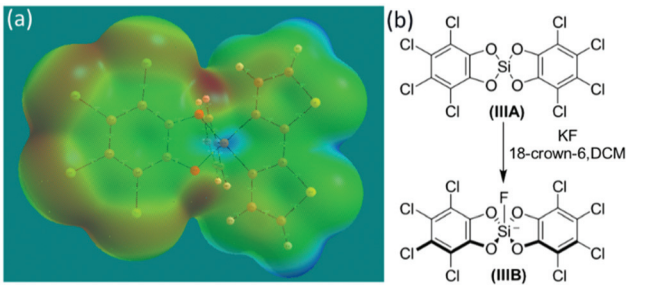

Fig. 3 (a) Electron density mapping showing the sigma hole in **A**; (b) silicon-based neutral Lewis acid.[12d]

Consequently, we were interested in the FIAs[25] of the new pentacoordinate dithienophospholes of this series to determine the Lewis acidity of the hypervalent P center. The calculated FIAs for compounds **B**, **A**, **D**, and **C** (gas phase) are 306, 334, 348, and 381 KJ mol^{-1} in increasing order (compared to the isodesmic reaction $Me_3SiF^- \rightarrow Me_3Si^+ + F^-$), respectively, that are correlated with the electron-withdrawing effects of both the *o*-chloranil and perfluorophenyl groups; the latter at the axial position has an expectedly stronger impact on enhancing the FIA. However, while the phosphorus center in these compounds is Lewis acidic, clearly none of the new hypervalent species are Lewis Super Acids. It is noteworthy, however, that the FIA values for **A–D** are significantly higher than that of the isoelectronic (**IIIB**) (71 KJ mol^{-1}).[12d] This highlights the effect of their neutral character in contrast to the anionic nature of (**IIIB**) with its already present fluoride substituent.

Fluoride abstraction reaction. With the computational data suggesting moderate Lewis acidity, we followed up with fluoride abstraction experiments. Compound **A** was initially reacted with one equivalent of potassium fluoride (KF) in dry toluene, but the $^{31}P\{^1H\}$ NMR spectrum of the reaction mixture after one hour confirmed the formation of compound **3** instead of $K^+[\mathbf{A}\text{–}\mathbf{F}^-]$. Similarly, the reaction of **A** with one equivalent of tetrabutylammonium fluoride (TBAF) showed weak doublets with ^1J(P–F) coupling for $TBA^+[\mathbf{A}\text{–}\mathbf{F}^-]$ ($^1J_{P-F} \sim 780$ Hz)[15b] after one hour of reaction time, but with **3** as the major product. The results were overall inconclusive regarding the Lewis acidity of this series of compounds, but suggested a different reaction was clearly occurring, at least for compound **A** (Scheme 2; ESI, section S3†).

Solvatochromism study of compound A. Due to the polar nature of its scaffold (as well as the presence of the sigma hole), we surmised that compound **A** would exhibit solvatochromism. Solutions of **A** ($c = 10^{-4}$ M) in DCM and toluene showed an absorption maximum λ_{max} = 388 nm that is blue-shifted to 358 nm in coordinating solvents such as acetone, THF, and acetonitrile (Fig. 4). The change in λ_{max} was accompanied by a change in solution color from yellow in toluene (and DCM) to colorless in coordinating solvents, indirectly supporting the Lewis acidity of **A** (see ESI, section 4†).

Reactivity with water. The fluoride abstraction studies suggested that presence of trace amounts of water trigger the transformation of **A** to **3** by a nucleophilic addition,[19] rather than a simple retro-[4 + 1] cycloaddition to the starting phosphole **1**. Notably, a solution of **A** in THF that was rigorously

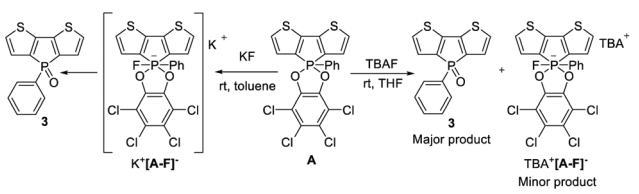

Scheme 2 Transformation of **A** to **3** *via* fluoride abstraction reaction.

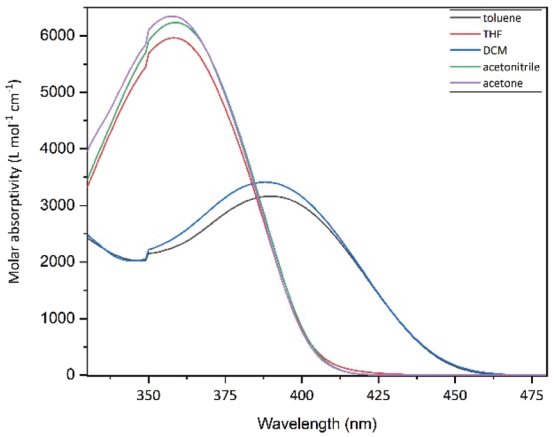

Fig. 4 UV-vis spectra of **A** in coordinating (THF, acetonitrile, and acetone) and non-coordinating (toluene and DCM) solvents.

dried over neutral alumina and freeze-pump-thawed, does indeed not show any formation of **3** by $^{31}P\{^1H\}$ NMR spectroscopy (ESI, section 4†). To further verify the adventitious water hypothesis, compound **A** was exposed to a controlled quantity of water in solution. Upon addition of 50% degassed water to a similarly dried THF solution of **A**, its blue-green fluorescence quickly changed to the bright blue emission characteristic of dithienophosphole oxide **3** (Fig. 5a). The formation of **3** was further confirmed by a downfield shift of the $^{31}P\{^1H\}$ NMR signal from −39.4 ppm for **A** (THF) to 13.9 ppm for **3** (THF/H_2O) (see ESI†). While compound **3** was clearly identified by NMR spectroscopy, the nature of the $C_6Cl_4O_2$-fragment, however, was unclear due to the ambiguity of the $^{13}C\{^1H\}$ NMR spectroscopic data.

Intriguingly, the rod-shaped golden yellow crystals of **A**, when left on the bench and exposed to atmospheric moisture in a loosely closed vial, transformed into pale yellow hexagonal crystals after two weeks, yet maintained suitable single-crystal characteristics for XRD analysis (Fig. 5b). X-ray crystallography on the transformed crystals confirmed the formation of phosphole oxide (**3**) with 3,4,5,6-tetrachloro-1,2-benzenediol (**4**) as the other by-product (Fig. 5c; ESI†). On the contrary to reactions happening exclusively on the surface, *i.e.*, the direct interface with the atmospheric moisture, the crystals are completely transformed to **3** and **4** showing that the decomposition of the outer layer opens the core of the unreacted crystal to a cascade of reactions. Notably, the crystallinity is preserved even as entropy increases. While the hydrolysis of P(v) catecholates is not unknown,[10e,26] the intriguing crystal-to-crystal transformation suggests that the corresponding mechanism for **A** may not necessarily require the breaking of a P–O catecholate bond (*vide supra*) as the initial step.

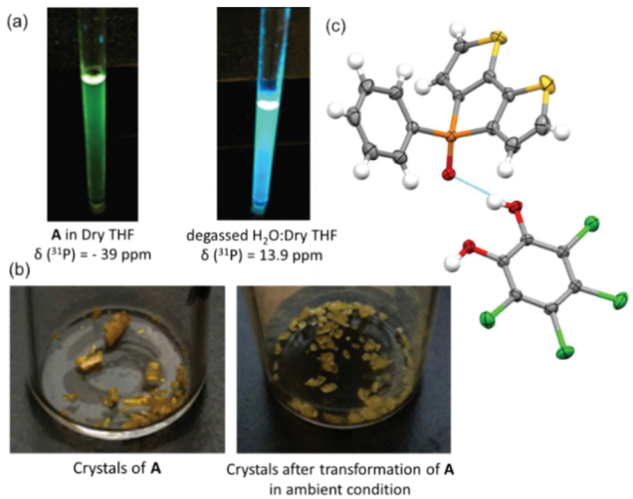

Fig. 5 (a) Solution-phase transformation; (b) crystal-to-crystal transformation; (c) products **3** and **4** of the crystal-to-crystal transformation (**A**·H_2O).

To gain more insights into the detailed mechanism of the reaction with water in general, we again turned our focus to computational chemistry. We first focused on the reaction in solution. The calculations employ a THF solvent model with one explicit THF molecule coordinated to H_2O *via* a hydrogen bond. The whole reaction is calculated to be exoergic by 20.0 kcal mol^{-1}, and there is essentially only one 20.3 kcal mol^{-1} barrier (**TS1**), which is feasible to overcome at room temperature (see ESI†). This rate-determining step involves concerted migrations of four electron pairs (Fig. 6a): (1) the addition of a H_2O lone pair to the acidic P center, forming the new O–P bond; (2) the heterolytic breakage of one original quinone O–P bond and the transfer of the bond electrons to the O atom; (3) this O atom donating its lone pair to a proton of the H_2O molecule to form an OH bond; and (4) heterolytic breakage of one OH bond in H_2O (see ESI for more details†).

In our experiments, alteration of the electronegativities of the axial group (C_6H_5 *vs.* C_6F_5) and the side group (chloranil *vs.* phenanthrene quinone) did not indicate a clear trend of reaction rates. Logic dictates that an electronegative axial group favors electron pair migration (1) but disfavors (2). An electronegative side group favors (2) but disfavors (3). The stochastic rates of the transformation of **A**, **C**, and **D** are reflections of these contradictory features. Once the H_2O-addition intermediate (**IM1**, Fig. 6b) is formed, the subsequent steps (in essence, second O–P breakage and proton transfer) are all thermodynamically and kinetically favorable (see Fig. S28(a) in ESI†). In the whole process, the phosphorus atom acts as a Lewis acid in electron pair migrations (1) and (5) and the aryloxy oxygen atom acts as a Lewis base in (3). The calculations show that an essentially similar mechanism is also

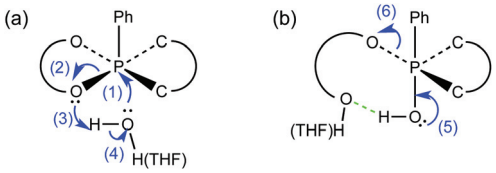

Fig. 6 Concerted electron-pair migrations for the reaction with water.

applicable to the solid-state transformation of the crystals of **A** in the presence of water (see Fig. S28(b) in ESI†). This proposed mechanism is uniquely supported by our observed reactivity, as the typical alternate reaction, requiring the breakage of a P–O bond first, instead of the acidity of the phosphorus center, relies on the basicity or electron-withdrawing nature of the substituent of which the O–P bond is broken, dictating a more intuitive ordering of the rates of transformation.[17a,c]

Supramolecular stabilization of the hypervalent compounds

Despite the Lewis acidity of the phosphorus center and the resulting increased reactivity to trace amounts of water, these kinetically labile compounds can nonetheless be crystallized from a concentrated solution on the bench. We assumed that their stability in the crystalline state would likely arise from intermolecular stabilization effects, given the fairly planar scaffold that allows for π–π interactions. The crystal packing of **A** shows molecules arranged in a parallel conformation where the exposed P center of one molecule is protected by the plane of a second molecule (3.5 Å) (Fig. 7a). Similar π–π interactions were also observed in single crystals of compounds **B** and **C**, while **D** forms π-stacked tetramers, likely due to the presence of both highly electron-withdrawing and -donating groups that complement each other intermolecularly (see ESI†).

The supramolecular dimerization interaction provides kinetic stability (at least for the medium term and the absence of nucleophiles), while the close intermolecular distance may afford electronic transitions across the dimers. To investigate both this, as well as the fate of these dimers in the solution state, the luminescence of these emissive compounds was studied as a function of concentration in dry toluene.

Notably, the interactions were found to be considerably strong, as excimer-type emissions[27] were observed, even at concentrations as low as 10^{-13} M. The excimer of compound **A** emits at 459 nm, while lowering the concentration to 10^{-7} M revealed a peak with vibronic structure centered around 409.5 nm that can be assigned to the monomeric species (Fig. 7b; we were able to exclude Raman scattering for these peaks by varying the excitation wavelength). Similarly, the monomer for compound **B** is detected at 396.5 nm (ESI†).

Compound **C** does not show clear monomer peaks even at a concentration of 10^{-6} M, which indicates extremely strong supramolecular interaction due to the increased Lewis acidity of the P(v) center hosting two highly electron-withdrawing substituents (Fig. 7c; here, the peak at 450 nm corresponds to Raman scattering). As already suggested by its solid-state structure, compound **D** also behaves differently in solution. The emission spectrum resolves into multiple peaks on dilution, as several different π–π interactions may persist, while exhibiting aggregation caused quenching (ACQ)[28] (ESI, section 5†).

Revisiting the fluoride abstraction reaction

As the initial fluoride abstraction reactions using typical fluoride salts ultimately led to the formation of **3** in all cases (Scheme 2), we concluded that this was due to the presence of adventitious water (*vide supra*). To eliminate this scenario, tris

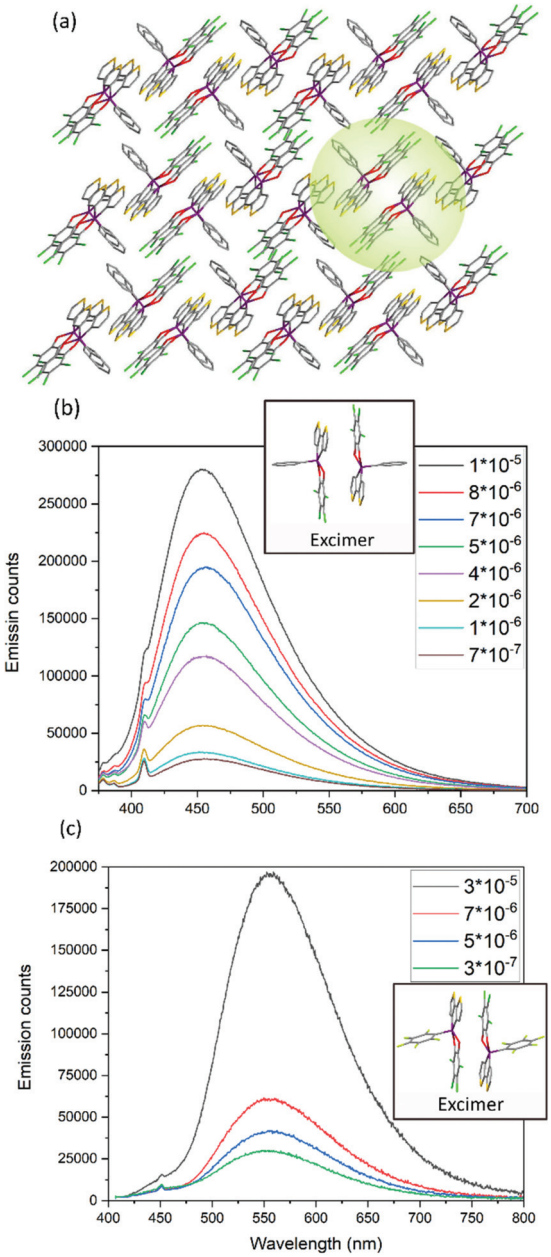

Fig. 7 (a) Crystal packing in **A** showing supramolecular π-stacked dimers; (b) fluorescence emission spectra showing monomer and excimer for **A** (excitation at 365 nm); (c) fluorescence emission spectra showing only excimers in **C** (excitation at 397 nm).

(dimethylamino) sulfur (trimethylsilyl) difluoride (**5**) was employed as a dry fluoride source for the anion abstraction reaction.[12d] Reactions of one equivalent of **5** with the hypervalent compounds **A–D** in meticulously dried solvent under argon, after one hour each give rise to highfield-shifted $^{31}P\{^1H\}$ NMR doublets with strong P–F coupling (as corroborated by $^{19}F\{^1H\}$ NMR spectroscopy). The shifts are consistent with octahedral P(v) species, and align well with related systems in the literature (Scheme 3).[29] Coupling constants ($^1J_{P-F}$) of 776 Hz (**A–F**$^-$), 752 Hz (**B–F**$^-$), 795 Hz (**C–F**$^-$), and 764 Hz (**D–F**$^-$),

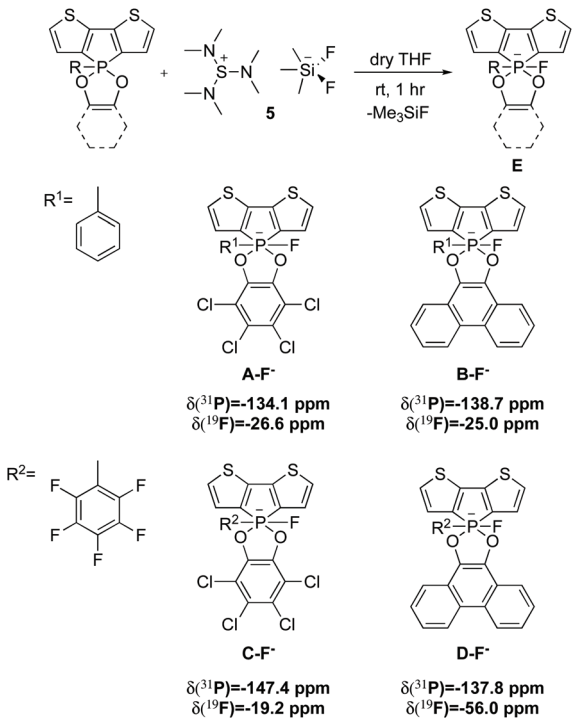

Scheme 3 Fluoride abstraction using 5 as dry source.

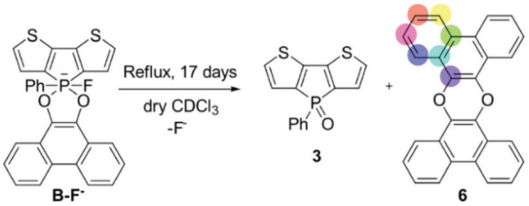

Scheme 4 Transformation of B–F$^-$ by deoxyaryloxylation reaction.

respectively, confirm the abilities of the pentavalent molecules to expand their coordination sphere to generate hexacoordinate species that are indeed reasonably stable under inert conditions.[15b,19,29,30]

Notwithstanding, also within one hour of reaction time, we observed the additional formation of a noticeable amount of dithienophosphole oxide **3** (or its C_6F_5-substituted relative **2-O**) by $^{31}P\{^1H\}$ NMR spectroscopy, along with the fluoride adducts (ESI, section 6†).

Despite the anaerobic conditions under which the fluoride abstraction reactions were conducted, the presence of dithienophosphole oxide suggests that further reactions beyond that of the fluoride abstraction must occur. This also indicated a fleeting nature for the corresponding fluoride adducts. Importantly however, given that there is no available external oxygen source for the formation of **3** (or its C_6F_5-substituted relative), the reaction pathway for this transformation must be clearly distinct from the one observed in the presence of water. Reaction of **5** with **B** shows the formation of **B–F**$^-$ and **3** after one hour in the $^{31}P\{^1H\}$ NMR spectrum in a roughly 11 : 7 ratio (see ESI, section 6†). The reaction mixture was then refluxed for 17 days to fully convert **B–F**$^-$ into **3**. After completion, the $^{13}C\{^1H\}$ NMR spectrum of the reaction mixture was recorded to establish the fate of the former phenanthrene quinone unit (see ESI†). In addition to the eight peaks for **3**, seven other peaks suggested the presence of a symmetric, 9,10-dioxo-phenanthrene fragment (Scheme 4 and ESI†). The anaerobic reaction conditions imply that the P=O unit of **3** must have been formed by breaking a C–O bond of **B–F**$^-$. There is precedence for a similar oxygen-transfer reaction in the literature, but the authors were unable to determine the fate of the corresponding diolate subsituent.[19a]

Given the highly symmetric nature of the phenanthrene-based moiety that was confirmed *via* $^{13}C\{^1H\}$ and ^1H NMR spectroscopy after its separation (see ESI†), formation of diphenanthro[9,10-*b*:9′,10′-*e*][1,4]dioxin (**6**) is the only plausible outcome for this reaction. The observed reaction could then be classified as an double deoxyaryloxylation, where one of the quinone oxygen atoms is transferred to phosphorus while the remaining forms an ether bond between the aryl groups. This intriguing observation indicates the potential utility of the new species as mediator in other organic transformations.[31,32]

To lend more credence to this proposed reaction, we again turned to computational chemistry using compound **A** as representative species for determination of a suitable reaction mechanism. The mechanism of the deoxyaryloxylation reaction is shown in Fig. 8. The first step is the abstraction of F$^-$ from **5** by **A**. This step is barrierless and exoergic by 8.7 kcal mol^{-1}. The abstraction results in a hexacoordinate compound **IM5** that aligns with the experimental observations (*vide supra*). Subsequently, **IM5** undergoes heterolytic O–P bond breakage to return to the pentacoordinate **IM6**, whose dangling O$^-$ is stabilized by the $[S(NMe_2)_3]^+$ countercation. The barrier for this step (**TS3**) is calculated to be 7.2 kcal mol^{-1}. Compared to the addition of H_2O to **A** (**TS1** in Fig. S26a, ESI†), only the migration arrows (2) and (3) are applicable here, and the barrier is lower by two thirds (vs. 20.3 kcal mol^{-1} of **TS1**). This is because: (1) the hexacoordinate phosphorus center with formal −1 charge in **IM5** has a stronger tendency to break the O–P bond and release the charge to the more electronegative oxygen center; (2) the $[S(NMe_2)_3]^+$ countercation is readily available to stabilize the anionic oxide. Both aspects are prototypical for the reactivity of octahedral P(v) catecholates.[33] Without the rigid ∼90° O–P–O bite angle, the pentacoordinate **IM6** adopts a 3BP structure, consistent with the discussion above, and described in more detail in the ESI (section 9).† An *ipso*-C atom of the dithieno-unit and the most electronegative fluoride occupy the axial positions. In the third step, electron pair migrations (10) and (11) occur in concerted fashion between a dimer of **IM6**; the remaining P–O–C unit is broken across the O–C bond in order to form a new O–C bond across the two *o*-chloranil groups. Since it is computationally costly to search for the transition state (**TS4**) for this large reaction complex, we estimate the barrier to be about 34.0 kcal mol^{-1}

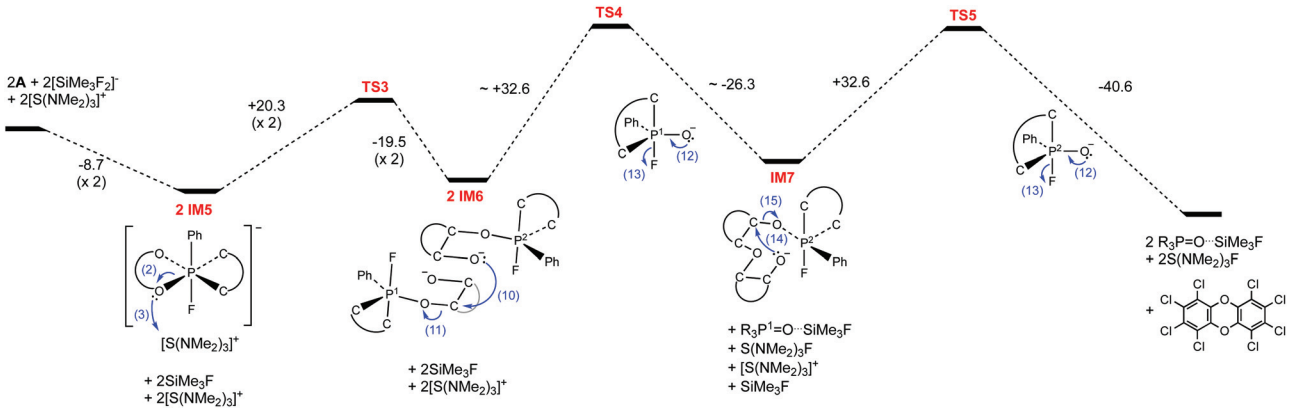

Fig. 8 Energy landscape for the deoxyaryloxylation reaction of **A**. In this figure two curves are used to schematically represent the *o*-chloranil and dithieno groups for better clarity. When necessary, the two carbon atoms connected to oxygen in the *o*-chloranil group are explicitly shown, while the other atoms of the group are omitted for clarity. Electron pair movements are shown in blue. Key structures are shown in Fig. S29 (ESI).† Energy differences between structures connected by dashed lines are given in kcal mol^{-1}. The energies for the first two dashed lines are for each **A** unit, while the others are for the whole system with two **A** units. The "x 2" suggests that the given energies are for each **A** unit and should be multiplied by two for the total system with two **A** units. **IM** and **TS** are numbered consecutively for all mechanism studies. **IM1–4** and **TS1–2** are shown in section 9 of ESI† for **A** + H_2O reaction mechanism. Similarly, details on pair migrations (1)–(9) are provided in section 9 of the ESI.† The energies were obtained using CAM-B3LYP/MA-DEF2-SVP/CPCM(THF) calculations and with zero-point energy corrections.

without running the search (*vide infra*). The barrier-less pair migrations (12) and (13) convert the pentacoordinate anion of P^1 (the two P atoms are labelled as P^1 and P^2 in Fig. 8 for better clarity) to **3**, whose oxygen atom weakly coordinates to the Si atom of an $SiMe_3F$ molecule (shown as $R_3P{=}O{\cdots}SiMe_3F$, with a 1.9 kcal mol^{-1} binding energy), and release an F^- to the solution (shown as $S(NMe_2)_3F$). The product **IM7** of this step has a similar electronic structure as **IM6**, with a dangling O^- stabilized by $[S(NMe_2)_3]^+$. The difference between **IM6** and **IM7** is that the C_6Cl_4 unit has been replaced by the C_6Cl_4–O–C_6Cl_4 dimer. **IM7** then undergoes the concerted pair migrations (14) and (15) to form perchlorodibenzodioxin (the *o*-chloranil congener to **6**). The remaining pentacoordinate anion of P^2 undergoes barrier-less migrations (12) and (13) to form another molecule of **3** (also coordinated to $SiMe_3F$) and returns an F^- to the solution. The transition state for this step (**TS5**) was found to be 34.0 kcal mol^{-1} above **IM6**. Since the pair migrations (14) and (15) resemble (10) and (11), the barrier of **TS4** is expected to be similar to that of **TS5**. We thus estimated the energy of **TS4** to be about 34.0 kcal mol^{-1} (*vide supra*). However, one should note that this conjecture is for the activation energy. Considering that **TS4** is in a bimolecular interaction, while **TS5** is in a intramolecular interaction, the reduction of entropy would give a higher Gibbs free energy barrier for **TS4** than **TS5**. But this does not change the overall picture of the reaction, which is held as a mixture of **IM5** and **IM6** for a long time.

The proposed mechanism suggests F^- to act as a catalyst and is exoergic by 17.5 kcal mol^{-1}. However, the two >30 kcal mol^{-1} barriers severely slow down the process. Also, the reaction may be trapped at the first step of forming **IM5**, which is isoergic with the final product. In fact, the addition of **5** to **A** results in a long-lasting mixture of the fluorinated **IM5** and the final products **3** and perchloro dibenzodioxin for more than a month. Similarly, persistent mixtures are observed for **C** and **D** and for all the three species, the final products (−17.5, −20.9, −27.5 kcal mol^{-1} for **A**, **C**, and **D**, respectively) are slightly lower or even substantially higher in energy than **IM5** (−17.4, −29.9, −24.5 kcal mol^{-1} for **A**, **C**, and **D**, respectively), leading to the prolonged observation of **IM5** in solution. Compound **B** is the only species that undergoes a complete deoxyaryloxylation, since the fluorination is much less exoergic than the deoxyaryloxylation (−11.2 *vs.* −28.1 kcal mol^{-1}). This lowest exoergicity in fluorination among **A–D** is consistent with the least electronegative side and axial groups of **B**. Still, the two approx. 30 kcal mol^{-1} barriers of **TS4** and **TS5** are in line with the experimentally observed deoxyaryloxylation using **B** that took 17 days to complete.

The mechanism also relies on the dynamic nature of the geometric structure present in these species. The fluoride abstraction requires the available coordination site of the 4SQ phosphorus center. The subsequent P–O bond breaking is, again, not uncommon among octahedral P(v) catecholates as a means to optimize the three 3c–4e bonds present in the structure. The less favorable F–P–C bond drives the ring opening and the subsequent reactivity along with the thermodynamic stability of a tetrahedral P(v) oxide. The generation of **3** during the reaction with more typical fluoride ion sources is also readily explained *via* this mechanism. Instead of a simple competition between F^- and water reacting at the Lewis acidic phosphorus center, the decomposition occurs from **IM5**. Upon ring opening, the water reacts with the now accessible phosphorus center instead of either rebinding the catechol or generating the dimer **IM6**. This would explain the presence of both **IM5** and **3** in solution from these reactions, as well as the slow rate of hydrolysis.

Conclusions

A facile method toward hypervalent dithieno[3,2-*b*:2′,3′-*d*]-phospholes *via* the [4 + 1] cycloaddition of *ortho*-quinones to trivalent species is reported. Our approach alleviates the requirements for additional kinetic stabilization, as often observed in previously reported systems. The structure of the obtained pentacoordinate derivatives deviates from the VSEPR theory-dictated trigonal bipyramidal geometry to form square pyramidal molecules, that in turn create a well-exposed Lewis acidic phosphorus center, evident in the presence of a sigma hole. This structural preference arises from the shallow potential energy surface connecting the two types of structure, which respectively balance two intermediate 3c–4e bonds on the one side, and both a strong and a weak 3c–4e on the other side. While we do not and cannot strictly rule out steric constraints about the phosphorus center, through this series of compounds, we were able to establish a thermodynamic model of the restrictions on forming a λ^5-P(v) center with 4SQ geometry. Additionally, based on the limited Lewis acidity of these compounds, we can propose the constraints of this model on Lewis acidity: (i) the stability of dimers formed even in solution; (ii) the dynamic geometry of these structures due to the extremely low energy difference between 3BP and 4SQ geometries; and (iii) the alternative reactivity of these species upon reacting with the Lewis base. The latter potentially affords this series of compounds an alternate use in the synthesis of other organic molecules. We can ascribe its Lewis acidity to these properties arising from the competing electronic effects of the system, in which the favorability of one strong 3c–4e bond is in direct competition of the generation of two 3c–4e bonds. By understanding the difference between the phosphorus bonding in, for example catechol *versus* dithienophosphole, this model may allow for the specific generation of λ^5-P(v) species strictly with either 4SQ or 3BP geometries. This would in turn enable targeted reactivities by adjusting the favorability of one 3c–4e bond to be much stronger or weaker than, serendipitously, this series of compounds in which both geometries are nearly isoergic. The Lewis acidic character of the 4SQ phosphorus center imparts high electrophilicity to water. The ensuing rapid transformation of the pentacoordinate compounds to dithienophosphole oxide, and an intriguing crystal-to-crystal transformation can be ascribed to the unique reactivity of these compounds as well as the significance of the geometric state toward their reactivity. Despite their high electrophilicity, the peculiar geometry of these compounds allows for kinetic intermolecular stabilization by supramolecular interactions in the solid state under ambient conditions. Hexacoordinate P-species are accessible by fluoride abstraction, which reveals the potential of these derivatives to facilitate interesting organic transformations such as the deoxyaryloxylation reaction that involves a generally challenging C–O bond activation.[34] The synthesized class of hypervalent phosphorus compounds presents an innovative structural platform while hosting desirable chemical properties that showcase once more the intriguing opportunities arising from conjugated main group species. Consequently, these species may have the potential to be exploited as neutral and stable hypervalent main group catalysts (or mediators) in organic chemistry. Now with a model to design these uniquely reactive compounds in hand, we are currently looking into expanding the scope of application of these reactive species.

Conflicts of interest

There are no conflicts to declare.

Acknowledgements

Financial support by the Natural Sciences and Engineering Research Council of Canada (NSERC) and the Canada Foundation for Innovation is gratefully acknowledged. T.B. thanks the Canada Research Chairs program for support. T.Z. thanks Calcul Quebéc and Compute Canada for computational resources.

Notes and references

1 S. Ogawa, *Organic Electronics Materials and Devices*, Springer, Japan, 2015.
2 (*a*) M. Stolar and T. Baumgartner, *Phys. Chem. Chem. Phys.*, 2013, **15**, 9007; (*b*) M. Stolar and T. Baumgartner, *Chem. – Asian J.*, 2014, **9**, 1212; (*c*) T. Baumgartner and F. Jäkle*Main group strategies towards functional hybrid materials*, Wiley, Hoboken, 2018.
3 (*a*) T. Baumgartner, T. Neumann and B. Wirges, *Angew. Chem., Int. Ed.*, 2004, **43**, 6197; (*b*) C. Romero-Nieto and T. Baumgartner, *Synlett*, 2013, 920.
4 T. Baumgartner, *Acc. Chem. Res.*, 2014, **47**, 1613.
5 Z. Wang, N. Asok, J. Gaffen, Y. Gottlieb, W. Bi, C. Gendy, R. Dobrovetsky and T. Baumgartner, *Chem*, 2018, **4**, 2628.
6 (*a*) Y. Ren, W. H. Kan, M. A. Henderson, P. G. Bomben, C. P. Berlinguette, V. Thangadurai and T. Baumgartner, *J. Am. Chem. Soc.*, 2011, **133**, 1701; (*b*) Y. Ren and T. Baumgartner, *Inorg. Chem.*, 2012, **51**, 2669.
7 (*a*) C. Y. Wong, D. K. Kennepohl and R. G. Cavell, *Chem. Rev.*, 1996, **96**, 1917; (*b*) V. Iaroshenko, *Organophosphorus Chemistry: From Molecules to Applications*, Wiley-VCH, Weinheim, Germany, 2019.
8 F. H. Osman and F. A. El-Samahy, *Chem. Rev.*, 2002, **102**, 629.
9 (*a*) J. F. Berry, *Dalton Trans.*, 2012, **41**, 700; (*b*) M. L. H. Green and G. Parkin, *Dalton Trans.*, 2016, **45**, 18784; (*c*) S. Noury and B. Silvi, *Inorg. Chem.*, 2002, **41**, 2164; (*d*) C. R. Landis and F. Weinhold, *Inorg. Chem.*, 2013, **52**, 5154.
10 (*a*) J. A. Howard, D. R. Russell and S. Trippett, *J.C.S. Chem. Commun.*, 1973, **1306**, 856; (*b*) R. R. Holmes and J. A. Deiters, *J. Am. Chem. Soc.*, 1977, **99**, 3318; (*c*) W. Althoff, R. O. Day, R. K. Brown and R. R. Holmes,

Inorg. Chem., 1978, **17**, 3265; (*d*) S. Sase, N. Kano and T. Kawashima, *J. Org. Chem.*, 2006, **71**, 5448; (*e*) M. Kaupp, *Angew. Chem., Int. Ed.*, 2001, **40**, 3534; (*f*) T. E. Clark, R. O. Day and R. R. Holmes, *Inorg. Chem.*, 1979, **18**, 1653; (*g*) T. E. Clark, R. O. Day and R. R. Holmes, *Inorg. Chem.*, 1979, **18**, 1660; (*h*) T. E. Clark, R. O. Day and R. R. Holmes, *Inorg. Chem.*, 1979, **18**, 1668; (*i*) H. R. Allcock and E. C. Bissell, *J. Am. Chem. Soc.*, 1973, **95**, 3154.

11 R. R. Holmes, *Acc. Chem. Res.*, 1979, **12**, 257.

12 (*a*) K. B. Dillon, R. N. Reeve and T. C. Waddington, *J. Chem. Soc., Dalton Trans.*, 1978, 1465; (*b*) L. A. Mück, A. Y. Timoshkin and G. Frenking, *Inorg. Chem.*, 2012, **51**, 640; (*c*) V. Fasano, J. H. W. LaFortune, J. M. Bayne, M. J. Ingleson and D. W. Stephan, *Chem. Commun.*, 2018, **54**, 662; (*d*) R. Maskey, M. Schädler, C. Legler and L. Greb, *Angew. Chem., Int. Ed.*, 2018, **57**, 1717; (*e*) H. Ruppert and L. Greb, *Organometallics*, 2020, **39**, 4340.

13 (*a*) P. J. Wheatley, *J. Chem. Soc.*, 1964, 3718; (*b*) A. L. Beauchamp, M. J. Bennett and F. A. Cotton, *J. Am. Chem. Soc.*, 1968, **90**, 6675; (*c*) M. A. García-Monforte, P. J. Alonso, I. Ara, B. Menjón and P. Romero, *Angew. Chem., Int. Ed.*, 2012, **51**, 2754; (*d*) R. R. Holmes, R. O. Day, V. Chandrasekhar and J. M. Holmes, *Inorg. Chem.*, 1987, **26**, 157; (*e*) R. R. Holmes, R. O. Day, V. Chandrasekhar and J. M. Holmes, *Phosphorus, Sulfur Silicon*, 1995, **99**, 13; (*f*) T. T. Bamgboye, M. J. Begley and D. B. Sowerby, *J. Organomet. Chem.*, 1989, **362**, 77; (*g*) A. P. M. Robertson, N. Burford, R. McDonald and M. J. Ferguson, *Angew. Chem., Int. Ed.*, 2014, **53**, 3480; (*h*) B. Pan and F. P. Gabbai, *J. Am. Chem. Soc.*, 2014, **136**, 9564.

14 Y. Ren, Y. Dienes, S. Hettel, M. Parvez, B. Hoge and T. Baumgartner, *Organometallics*, 2009, **28**, 734.

15 (*a*) P. Narayanan, H. M. Berman, F. Ramirez, J. F. Marecek, Y. Chaw and V. A. V. Prasad, *J. Am. Chem. Soc.*, 1977, **99**, 3336; (*b*) M. Koenig, A. Klaebe, A. Munoz and R. Wolf, *J. Chem. Soc., Perkin Trans. 2*, 1979, 40.

16 (*a*) T. S. Cameron and B. Dahlén, *J. Chem. Soc., Perkin Trans. 2*, 1975, 1737; (*b*) J. A. Dobado, H. Martínez-García, J. M. Molina and M. R. Sundberg, *J. Am. Chem. Soc.*, 1998, **120**, 8461.

17 (*a*) J. Lacour and A. Londez, *J. Organomet. Chem.*, 2002, **643**, 392; (*b*) J. Lacour, A. Londez, D. Tran, V. Desvergnes-Breuil, S. Constant and G. Bernardinelli, *Helv. Chim. Acta*, 2002, **85**, 1364; (*c*) J. Lacour, C. Ginglinger, C. Grivet and G. Bernardinelli, *Angew. Chem., Int. Ed.*, 1997, **36**, 608.

18 J. C. Gilhula and A. T. Radosevich, *Chem. Sci.*, 2019, **10**, 7177.

19 (*a*) F. Ramirez, V. A. V. Prasad and J. F. Marecek, *J. Am. Chem. Soc.*, 1974, **96**, 7269; (*b*) S. Trippett and R. E. L. Waddling, *Tetrahedron Lett.*, 1979, **20**, 193.

20 R. R. Holmes, *J. Am. Chem. Soc.*, 1975, **97**, 5379.

21 J. P. Foster and F. Weinhold, *J. Am. Chem. Soc.*, 1980, **102**, 7211.

22 Y. Lin, J. C. Gilhula and A. T. Radosevich, *Chem. Sci.*, 2018, **9**, 4338.

23 T. A. Keith, *AIMAll (Version 19.10.12), TK Gristmill Software*, Overland Park KS, USA, 2019, (aim.tkgristmill.com).

24 J. Y. C. Liam and P. D. Beer, *Chem*, 2018, **4**, 731.

25 (*a*) L. Greb, *Chem. – Eur. J.*, 2018, **24**, 17881; (*b*) J. Zhou, L. L. Liu, L. L. Cao and D. W. Stephan, *Angew. Chem., Int. Ed.*, 2019, **58**, 5407.

26 (*a*) R. R. Holmes, *Chem. Rev.*, 1996, **96**, 927; (*b*) P. G. Mashaffy, J. D. Wieser and L. K. Montgomery, *J. Am. Chem. Soc.*, 1977, **99**, 4515; (*c*) P. W. Siu and D. P. Gates, *Organometallics*, 2009, **28**, 4491; (*d*) T. Kawashima, R. Okazaki and R. Okazaki, *Angew. Chem., Int. Ed. Engl.*, 1997, **36**, 2500.

27 J. R. Lakowicz, *Principles of Fluorescence Spectroscopy*, Kluwer Academic/Plenum, New York, 1999.

28 R. Jakubiak, C. J. Collison, W. C. Wan and L. J. Rothberg, *J. Phys. Chem. A.*, 1999, **103**, 2394.

29 (*a*) T. Kaukorat, P. G. Jones and R. Schmutzler, *Heteroat. Chem.*, 1991, **2**, 81; (*b*) J. A. Gibson, G. Roschenthaler and R. Schmutzler, *J. Chem. Soc., Dalton Trans.*, 1975, 918.

30 (*a*) A. F. Janzen, *Coord. Chem. Rev.*, 1994, **130**, 355; (*b*) M. Gallagher, *J. Chem. Soc., Chem. Commun.*, 1976, 321; (*c*) J. J. H. M. Font Freide and S. Trippett, *J. Chem. Soc., Chem. Commun.*, 1980, 157.

31 (*a*) A. E. Waked, S. S. Chitnis and D. W. Stephan, *Chem. Commun.*, 2019, **55**, 8971; (*b*) T. Stahl, H. F. T. Klare and M. Oestreich, *ACS Catal.*, 2013, **3**, 1578; (*c*) P. Spies, G. Erker, G. Kehr, K. Bergander, R. Fröhlich, S. Grimme and D. W. Stephan, *Chem. Commun.*, 2007, 5072; (*d*) R. Dobrovetsky, K. Takeuchi and D. W. Stephan, *Chem. Commun.*, 2015, **51**, 2396; (*e*) M. C. Hilton, X. Zhang, B. T. Boyle, J. V. Alegre-Requena, R. S. Paton and A. McNally, *Science*, 2018, **362**, 799; (*f*) N. Đorđevic, M. Q. Y. Tay, S. Muthaiah, R. Ganguly, D. Dimić and D. Vidović, *Inorg. Chem.*, 2015, **54**, 4180; (*g*) D. W. A. Stephan, *Angew. Chem., Int. Ed.*, 2017, **56**, 5984.

32 (*a*) J. J. Jennings, B. W. Wigman, B. M. Armstrong and A. K. Franz, *J. Org. Chem.*, 2019, **84**, 15845; (*b*) J. M. Bayne and D. W. Stephan, *Chem. Soc. Rev.*, 2016, **45**, 765; (*c*) S. Postle, V. Podgorny and D. W. Stephan, *Dalton Trans.*, 2016, **45**, 14651.

33 (*a*) A. Munoz, M. Gallagher, A. Klabe and R. Wolf, *Tetrahedron Lett.*, 1976, **9**, 673; (*b*) F. Ramirez, M. Nawakowski and J. F. Marecek, *J. Am. Chem. Soc.*, 1977, **99**, 4515.

34 (*a*) K. E. Torraca, X. Huang, C. A. Parrish and S. L. Buchwald, *J. Am. Chem. Soc.*, 2001, **123**, 10770; (*b*) M. Palucki, J. P. Wolfe and S. L. Buchwald, *J. Am. Chem. Soc.*, 1997, **119**, 3395.

